PAPER

Check for updates

ZnO films using a precursor solution irradiated with an electron beam as the cathode interfacial layer in inverted polymer solar cells†

Rira Kang,[a] Yong-Jin Noh,[b] Jin-Mun Yun,[a] Hyun Kim,[a] NoSoung Myoung,[d] Eun-Hye Lee,[c] Tae-Wook Kim, [c] Seok-In Na ‡*[b] and Seung-Hwan Oh ‡*[a]

We demonstrate the possibility of irradiating sol–gel ZnO with an electron beam (**EB-ZnO**) to modify sol–gel ZnO, and **EB-ZnO** is explored as a cathode interfacial layer for inverted polymer solar cells. We investigate the effect of **EB-ZnO** on the surface, optical and electric properties of sol–gel ZnO films through morphology, chemical composition, optical band gap shift, various defect excitations (photoluminescence) and work function measurement. Oxygen vacancies and the formation of nitrogen on the surface of **EB-ZnO** films contribute to the formation of n-type degenerated **EB-ZnO** films. The electric properties of **EB-ZnO** strongly depend on the adsorbed dose, and **EB-ZnO** with a suitable dose of 100 kGy improved the power conversion efficiency of inverted polymer solar cells based on PTB7-Th: $PC_{71}BM$ from 8.05% for non-treated sol–gel ZnO to 9.36% for **EB-ZnO** with an enhanced fill factor.

Introduction

Polymer solar cells (PSCs) have attracted considerable attention due to their low cost, light weight, flexibility, environmentally friendly energy sources.[1–7] Various strategies (low band gap donors,[1,2] novel acceptors,[3,4] new device configurations,[5,6] and interface engineering[7,8]) have been rapidly developed to improve their power conversion efficiency (PCE). Recently, PSCs with low band gap donors have achieved PCE greater than 10%.[1,2] The inverted device configuration in polymer solar cells (ITO/cathode interfacial layer/active layer/anode interfacial layer/Ag) has been widely used due to its higher PCEs and longer lifetimes than that of the conventional configuration.[9]

In inverted PSCs, a cathode interfacial layer (CIL) such as metal oxide (ZnO, TiO_x and Cs_2CO_3) and conjugated polymers is required to change the polarity of ITO to a cathode.[7,10,11] Among them, sol–gel ZnO has been the most commonly used material

as a CIL due to its (1) high transparency, (2) suitable energy level (conduction band: −4.4 eV and valence band: −7.8 eV) for electron collection and hole blocking, (3) good electron mobility, and (4) easy solution processing.[10–12] However, the widely used sol–gel ZnO exhibits many surface defects/traps, such as dangling bonds and adsorbed oxygen on its surface due to low temperature solution processing.[11] Such defects act as recombination centers and lead to poor device performances in PSCs. To overcome these problems, many approaches such as control of morphology, modification of nanostructure, doping and surface modification with self-assembly layer or polymers bilayer have been developed for better electron collection.[10–12]

As a promising new approach, techniques based on various types of ionizing radiation (alpha, electron beam, gamma rays, X-rays, laser ablation, α-particles, neutrons, protons, and ion beams) for the fabrication and synthesis of materials are becoming useful.[13,14] The high energy of electron beam leads to the formation of radicals within a short time.[14] Especially, the effect of electron-beam irradiation on the electrical and optical properties of ZnO was recently investigated. K. P. Sapnar *et al.* synthesized ZnO nanoparticles (NPs) *via* microwave, and the ZnO NPs powder was exposed to electron irradiation, which resulted in an increase in their bandgap and reduction of the NPs size.[15] J. S. Bhat *et al.* observed an increase in sheet resistance, blue shift in the absorption edge and decrease in structural homogeneity and crystalline size after sol–gel ZnO and ZnO:Al films were exposed to electron irradiation.[16] The results of such research indicate that electron beam irradiation could induce defects and modify electronic and optical properties, regardless of the phase of ZnO (films or powder). However, to the best of our knowledge, the application of ZnO

aRadiation Research Division for Industry and Environment, Korea Atomic Energy Research Institute (KAERI), 29 Geumgu-gil, Jeongeup-si, Jeollabuk-do 580-185, Republic of Korea. E-mail: ohsh@kaeri.re.kr

bProfessional Graduate School of Flexible and Printable Electronics, Polymer Materials Fusion Research Center, Chonbuk National University, 664-14, Deokjin-dong, Jeonju-si, Jeollabuk-do 561-756, Republic of Korea. E-mail: nsi12@jbnu.ac.kr

cAdvanced Photonics Research Institute (APRI), Gwangju Institute of Science and Technology (GIST), Gwangju 61005, Republic of Korea

dSoft Innovative Materials Research Center, Institute of Advanced Composite Materials, Korea Institute of Science and Technology, Joellabuk-do 565-905, Republic of Korea

‡ These two authors are contributed equally to this work.

exposed to electron irradiation in solar cells has not yet been reported.

Hence, sol–gel ZnO irradiated with an electron beam was developed as a CIL in inverted polymer solar cells with a device structure of ITO/electron-beam based sol–gel ZnO (**EB-ZnO**)/PTB7-Th:PC$_{71}$BM/MoO$_3$/Ag. Herein, the application of **EB-ZnO** as a cathode interfacial in PSCs is first reported. We directly irradiate the sol–gel ZnO precursor solution with an electron beam as a function of adsorbed dose (100, 300 and 500 kGy), and use ZnO films spin-coated from the irradiated solution as a CIL in inverted PSCs. This electron irradiation makes the sol–gel ZnO n-type degenerated by inducing oxygen vacancies, which can increase electron concentrations; and their surface composition, morphology, photoluminescence, energy-level diagram are investigated to understand the fundamentals of the changed properties of **EB-ZnO**. The inverted PSCs with **EB-ZnO** at 100 kGy exhibit the best power conversion efficiency (PCE) of 9.36% due to the enhanced fill factor of 71.8%. In addition, the device with **EB-ZnO** at 100 kGy exhibits the lowest series resistance and dominant bimolecular recombination.

Experimental

Preparation of irradiated sol–gel ZnO with electron beam (EB-ZnO)

Sol–gel ZnO was prepared according to a previous report.[17] Next, 20 mL sol–gel ZnO in a glass vial was irradiated at room temperature with electron-beam irradiation at a scan rate of 10 kGy min^{-1} created by 2.5 MeV UELV-10-10S electron accelerator at the Korea Atomic Energy Research Institute (ex. 2.5 MeV × 5.8 mA × 10 m min^{-1} × 1 turn = 10 kGy). The total absorbed doses were 100, 300 and 500 kGy. The untreated sol–gel ZnO and sol–gel ZnO irradiated with electron beam at 100, 300 and 500 kGy are denoted as **Ref**, **EB-Z100**, **EB-Z300** and **EB-Z500**, respectively.

Fabrication and characterization of inverted polymer solar cells

To fabricate the device, ITO coated glass was cleaned with acetone, DI water and IPA, dried in an oven, and UV-ozone treated for 20 min. **EB-ZnO** was spin-coated onto ITO, at a thickness of ∼60 nm, followed by drying at 150 °C for 30 min under air. As the active layer, a blend solution film of 12 mg of PTB7-Th (1-material) and 18 mg of PC$_{71}$BM (1-material) in 1 mL of chlorobenzene with 5% (v/v) the additive DIO was then spin-coated onto **EB-ZnO** at 2000 rpm for 60 s in an N$_2$-filled glove box. Under the vacuum of 10^{-6} torr, 3 nm MoO$_3$ was thermally evaporated onto the active layer, and then 80 nm-thick silver as the anode electrode was thermally deposited onto MoO$_3$ through a shadow mask with an area of 4.64 mm^2. The photo-current–voltage (*J–V*) characteristics of the devices were measured using a Keithley 2400 instrument and solar simulator (Oriel sol3A) under air.

Sample characterization

Atomic force microscopy (AFM) (Veeco, Digital Instruments Nanoscope IIIA) in tapping mode was used to characterize the

EB-ZnO films spin-coated on Si wafers. X-ray photoelectron spectroscopy (XPS) and ultraviolet photoemission spectroscopy (UPS) measurements (AXIS NOVA, Kratos) were carried out for the **EB-ZnO** films spin-coated on ITO substrates (mono-chromatized Al Kα for XPS, and a He l (*hν* = 21.2 eV) excitation for UPS at a pressure of 5 × 10^{-8} torr). The UV-vis spectra of spin-coated **EB-ZnO** films spin-coated on glass substrates were recorded using a spectrophotometer. Photoluminescence (PL) spectra of **EB-ZnO** films spin-coated on glass substrates were measured *via* the 2nd harmonic generation (at 350 nm) of a mode-locked Ti:Sapphire laser (Chameleon Ultra II coherent) at 300 K. Transmission electron microscopy (TEM) was used to investigate the crystalline size of **EB-ZnO** (Titan 80-300, FEI, operated at 300 kV). For the characterization, the **EB-ZnO** films were prepared *via* the same procedures as that for device fabrication.

Result and discussion

Surface properties

Fig. 1a shows a photograph of the actual solutions of **Ref**, **EB-Z100**, **EB-Z300** and **EB-Z500**. With an increase in the adsorbed dose from 100 to 500 kGy, the color of the **EB-ZnO** solution changed from transparent to orange-red. To observe the differences in surface properties between all the samples, as shown in Fig. 1b, the morphologies of the **Ref** and **EB-ZnO** samples were investigated *via* atomic force microscopy (AFM). All the samples exhibit flat surfaces without a ripple type morphology, which is probably due to the low-temperature annealing. **EB-Z100** a slightly reduced surface roughness compared with that of **Ref**; whereas **EB-Z500** shows a rough surface with a random distribution of particles. The increase in surface roughness suggests that electrons cannot be collected beneficially to the cathode. To observe the change in the crystalline size of **EB-ZnO**, the **EB-ZnO** samples were characterized using TEM. Unexpectedly, there was no significant change in all the samples (crystalline size: about 0.23 nm in Fig. S1†).

In order to obtain information about the surface of **EB-ZnO**, XPS analysis was carried out on **EB-ZnO**. The binding energies were calibrated with respect to the C 1s peak at 258.0 eV. As
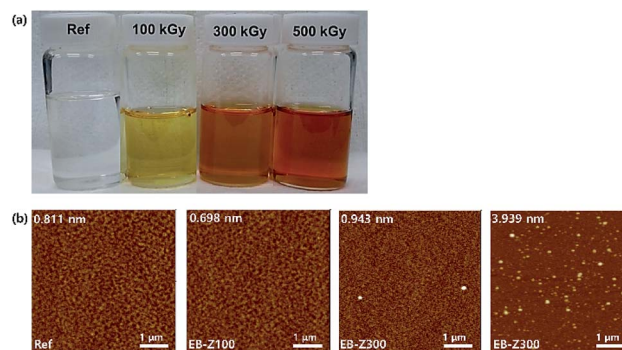

Fig. 1 (a) Photograph of the **Ref** and **EB-ZnO** precursor solutions and (b) AFM images of the **Ref** and **EB-ZnO** films with a size of 5 × 5 μm^2. The upper left value is the root-mean-square (RMS) in the AFM images.

shown in Fig. 2, the O 1s peaks can be deconvoluted into three Gaussian components (O_a: O^{2-} ions in the ZnO lattice, O_b: O^{2-} ions in the oxygen vacancy of ZnO and O_c: chemisorbed oxygen species on the surface of ZnO).[18] For better comparison, the content and peak positions of each O 1s component are shown in Fig. 2. The O 1s peaks of **Ref** are centered at 530.6 eV (O_a: 63.8%), 531.5 eV (O_b: 7.7%) and 531.9 eV (O_c: 28.5%). With the increase in the irradiation dose, the O 1s peaks broaden and shift toward lower binding energies by 0.4, 0.9 and 0.7 eV, and the content of O_b increases to 43.3%, 80.1% and 58.0% for **EB-Z100**, **EB-Z300** and **EB-Z500**, respectively. It is known that such oxygen vacancy can act as donors, which lead to degenerate ZnO by increasing the electron carrier density in the conduction band (CB) of ZnO. Moreover, the content of O_c decreases to 12.0%, 1.3% and 1.9% for **EB-Z100**, **EB-Z300** and **EB-Z500**, respectively. The surface hydroxyl groups trap photoinduced electrons and holes, thus enhancing the photocatalytic degradation process. It is noted that electron beam irradiation can induce oxygen vacancies and reduce surface hydroxyl groups of sol–gel ZnO.[34]

For all samples, Zn 2p has doublet peaks (for the non-treated ZnO, Zn $2p_{3/2}$: 1021.6 eV and Zn $2p_{1/2}$: 1044.7 eV). The Zn 2p peak shifts toward a lower binding energy by 0.4, 0.7 and 0.8 eV for **EB-Z100**, **EB-Z300** and **EB-Z500**, respectively, similarly to the shift of the O 1s peak. FWHM (full width at half maximum) can be an indicator of chemical state changes and physical influence. With the increase in irradiation dose, Zn 2p FWHM broadening occurs (**Ref**: 1.456, **EB-Z100**: 1.497, **EB-Z300**: 1.551 and **EB-Z500**: 1.776), and additional peaks are also observed at higher biding energies (the shaded area of the insets in Fig. 2). This result can be attributed to the presence of zinc interstitial (Zn_i).[19] It is reported that Zn_i can degenerate ZnO by acting as donors and can interact with adjacent active layers with respect to the stability of polymer solar cells.[35]

Interestingly, we also observed N 1s spectra in the **EB-ZnO** samples, but not in **Ref**. The N 1s of **EB-Z100** can be deconvoluted into two peaks at 398.1 and 399.7 eV, which are attributed to –C═N– and –NH–C or N–$(C)_3$, respectively.[20] Given the content of O_b for the **EB-ZnO** samples, it is expected that N atoms do not occupy the O sites in our study (*i.e.*, N–Zn bonds is not observed). The two peaks of **EB-Z300** and **EB-Z500** slightly shift toward lower binding energies, which contributes to the enhanced electron concentration of the modified **EB-ZnO** surface by the interaction between different types of amines and ZnO. Although the origin of N formation on the **EB-ZnO** surface is not clear, it can originate from the byproduct (NH_4^+) related to the degradation of ethanolamine[21] or unstable intermediate products such as OH· and H· radicals by electron beam irradiation.[13] It can be suggested that the byproducts, unstable intermediate products and reactants from the ZnO precursor solution, which are not volatile at 150 °C, are adsorbed on the surface of ZnO.

Optical properties

The optical properties of the samples were investigated, as shown in Fig. 3a and b. The band gaps (E_g) of **EB-ZnO** were estimated from the $(\alpha h\nu)^2$ *vs.* $h\nu$ plot (Tauc plot extrapolation). The band gap is estimated to be 3.33, 3.36, 3.38 and 3.37 eV for **Ref**, **EB-Z100**, **EB-Z300** and **EB-Z500**, respectively (refer to Table 2 and Fig. 2a). The absorption spectra of samples are presented in Fig. 2b. All the **EB-ZnO** samples show UV absorption and transparency in the visible region and with the increase in absorption dose, their band gaps increase. The **EB-Z500** sample is significantly blue shifted compared to the other samples. The band gap widening of the **EB-ZnO** samples is probably due to the well-known Burstein–Moss effect (BM effect), which is related to heavily doped/degenerated semiconductors. The BM
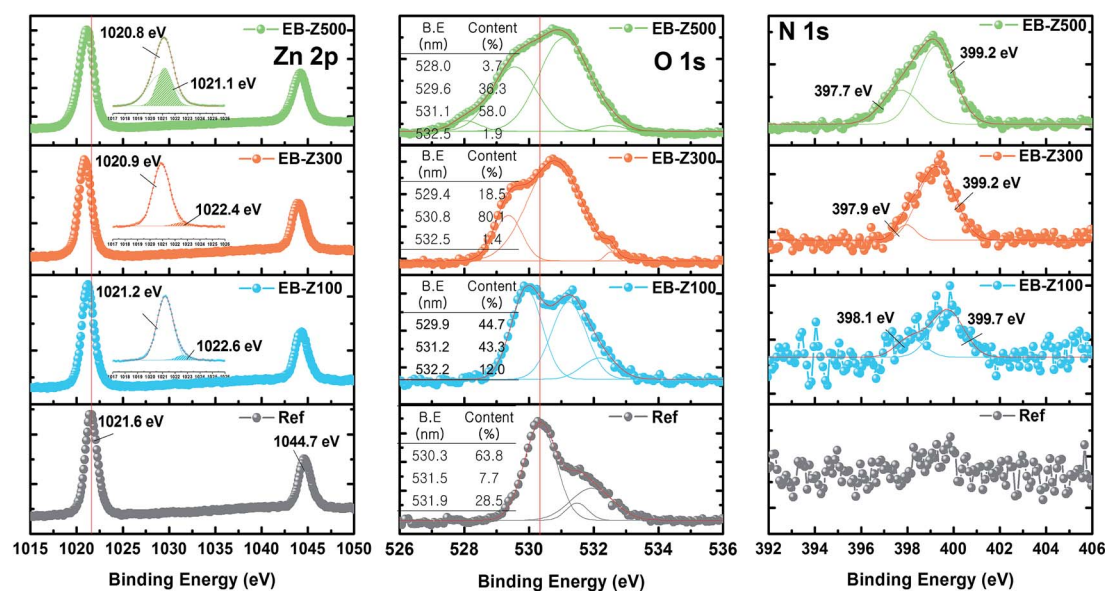

Fig. 2 Zn 2p, O 1s, and N 1s XPS spectra of **Ref**, **EB-Z100**, **EB-Z300** and **EB-Z500** (inset in the O 1s XPS spectra is the content of oxygen species calculated from O 1s fitting spectra).
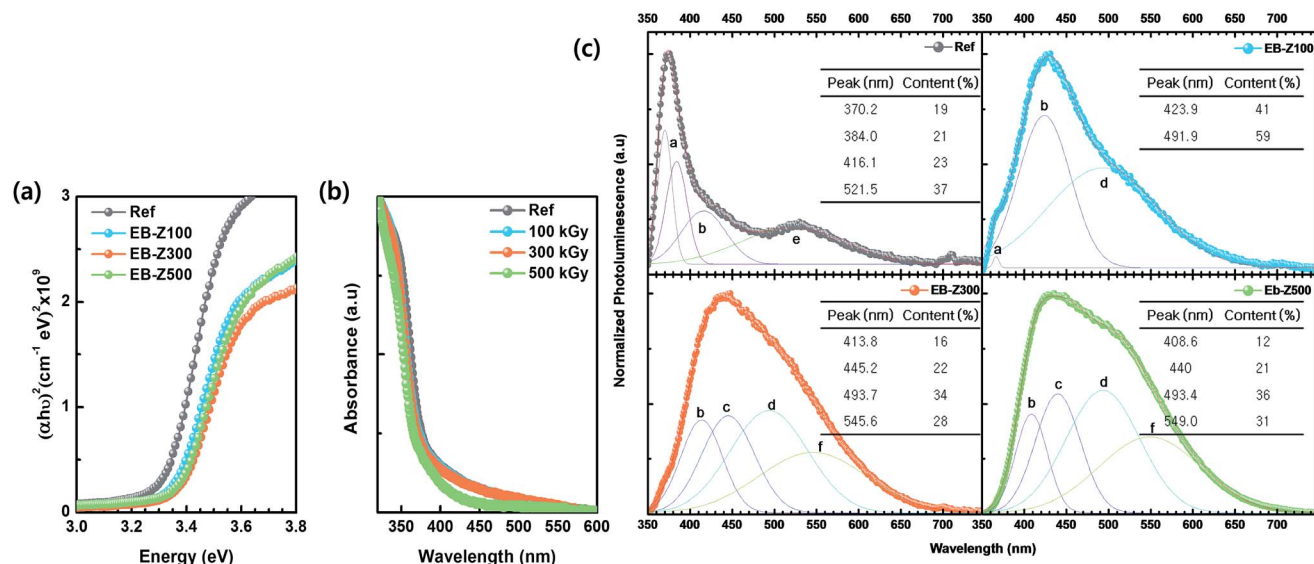
Fig. 3 (a) Tauc plot, (b) UV-vis spectra and (c) normalized photoluminescence (PL) spectra of **Ref**, **EB-Z100**, **EB-Z300** and **EB-Z500**. PL spectra were deconvoluted into Gaussian peaks (a to f correspond to Table 1 and Scheme 1).

Table 1 The spectral locations of the deconvoluted peaks and their possible emission mechanism

Related defects		Zn_i, V_{Zn}, O_i (nm, eV)		V_O (V_O^*)	O_{Zn}	O_i, V_O
Color	Interband (nm, eV)	Violet	Blue	Sky blue	Green	
Ref	370.2, 3.35	416.1, 2.98			521.5, 2.38	
	384.0, 3.23					
EB-Z100	—	423.9, 2.93		491.9, 2.52		
EB-Z300	—	413.8, 3.00	445.2, 2.78	493.7, 2.51		545.6, 2.27
EB-Z500	—	408.6, 3.03	440, 2.81	493.4, 2.51		549.0, 2.26
Possible mechanism	(a) $FX \rightarrow VB$ $CB \rightarrow VB$	(b) $CB \rightarrow V_{Zn}$ $Zn_i \rightarrow VB$ $CB \rightarrow O_i$	(c) $ex\text{-}Zn_i \rightarrow VB$	(d) $V_O^* \rightarrow VB$	(e) $CB \rightarrow O_{Zn}$	(f) $CB \rightarrow O_i$ $CB \rightarrow V_O$

effect is the phenomenon in which doping causes a Fermi level (E_f) shift above the conduction band, *i.e.* since electrons fill up all the states below E_f, the optical band gap increases.[22,23]

In addition, for the characterization of **EB-ZnO** defects, the photoluminescence (PL) spectra of samples are shown in Fig. 3c. The **Ref** sample shows both UV emission and visible emission and **EB-Z100** slightly shows UV emission, whereas the other **EB-ZnO** samples did not show UV emission (red-shifted PL) despite their blue-shifted UV-vis spectra. Such red-shifted PL spectra of **EB-ZnO** result from the fact that absorption occurs from the valance band to the E_f or the conduction band (CB), whereas luminescence occurs from the impurity-donor band to the valance band (VB) or acceptor-like state.[24] Since PL spectra are suitable tools for the characterization of the defects, the PL spectra were deconvoluted into several Gaussian subpeaks. Generally, there are a number of defect states within the bandgap of ZnO (donor defects: zinc interstitial, Zn_i, and oxygen vacancy, V_O, acceptor defects: zinc vacancy, V_{Zn}, oxygen

Table 2 The bandgap, valence band, conduction band and work function of values **Ref**, **EB-Z100**, **EB-Z300** and **EB-Z500**

	E_g (eV)	V.B (eV)	C.B (eV)	W.F (eV)
Ref	3.33	7.56	4.23	4.12
EB-Z100	3.35	7.54	4.19	3.75
EB-Z300	3.38	7.44	4.06	3.55
EB-Z500	3.37	7.44	4.07	2.99

interstitial, O_i and oxygen antisite, O_{Zn}). It is known that the relative content of donor and acceptors influences the semiconductor properties of ZnO.[25]

Scheme 1 and Table 1 show the various defects level emissions for the deconvoluted peaks (a to f) of the PL spectra (Fig. 3c). The origin of the PL spectra is complicated, which is due to the fact that PL is mostly related to V_O and/or Zn_i. As mentioned above, the **Ref** and **EB-Z100** samples only exhibit UV emission (peak a), which is due to that free excitons (FX, 0.06 eV
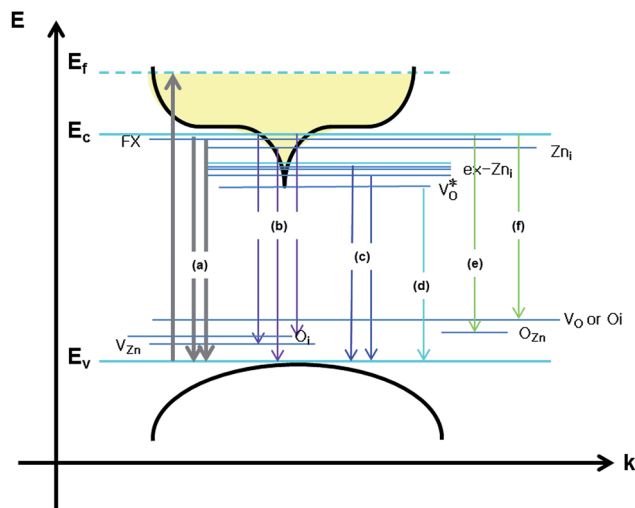
Scheme 1 Schematic diagram of the energy band structures of **EB-ZnO** and photoluminescence mechanism of **EB-ZnO** corresponding to the data in Table 1.

below the CB) recombine with holes in the VB.[26] With an increase in the absorption dose, the PL spectra display visible region broadening. The violet emission (peak b) displayed in all the samples is probably attributed to (1) Zn_i (about 0.22 eV below the CB) → VB transition or (2) CB → single ionized V_{Zn} (about 0.3 eV above the VB) or (3) CB → O_i (about 0.4 eV above the VB).[25–27] The blue emission (peak c) of **EB-Z300** and **EB-Z500** is due to ex-Zn_i, which is the extended states of Zn_i from 0.54 to 0.64 eV below the CB.[26,27] This can be correlated to the additional Zn 1p peaks of **EB-Z300** and **EB-Z500** (the shaded area, inset Fig. 2), where the shaded area of **EB-Z500** is significant (inset Fig. 2). For the **EB-ZnO** samples, the sky blue emission (peak d) results from the process ($V_O^* \rightarrow V_O^+ + e^-$, below the CB) in the grain boundary.[26] The increase in the content of O_b for the **EB-ZnO** samples is evidence of this emission. For only the **Ref** sample, electron transition from the CB to O_{Zn} occurs (peak e).[28] The green emission (peak f) of **EB-Z300** and **EB-500** is due to two possibilities: (1) CB → O_i (about 1.09 eV above the VB) or (2)

trap state emissions attributed to the single ionized V_O (about 0.90 eV above the VB).[27] The PL spectra of **EB-Z100** includes two subpeaks (b and d) related to donor defects (Zn_i and V_O^*), whereas that of **EB-Z300** and **EB-Z500** significantly include additional contents (lines d and f) related to both donor and acceptor defects (V_{Zn}, O_i and V_O). The origin of the PL emission does not seem to clearly correlate with the intrinsic or extrinsic defects due to the extremely complicated defect energy level. However, the presence of ex-Zn_i and V_O is supported by the XPS results, which indicates that oxygen vacancies and Zn interstitial are dependent on the irradiation dose.

Electronic properties

To observe the change in energy levels of the **EB-ZnO** samples, we carried out ultraviolet photoelectron spectroscopy (UPS) measurements (Fig. 4a). Fig. 4b and Table 2 exhibit the energy levels extracted from the UPS results. The work function (W.F, φ) is determined by the distance between the secondary electron edge at high binding energy and HeI energy = 21.2 eV (the left panel in Fig. 4a). The valence band maximum (VBM) was calculated from the onset to the E_f at the low binding energy region (the right panel in Fig. 4a). The conduction band minimum (CBM) was estimated from the VBM and E_g (extracted from the Tauc plot). The **Ref** samples show a W.F of about 4.12 eV, which is similar with that of previously reported sol–gel ZnO,[29] but an E_f slightly above the CB is observed in our study. With the increase in irradiation dose from 100, 300 to 500 kGy, the W.F decreases from 3.75, 3.55 to 2.99 eV, respectively. As mentioned for the bandgap widening of the **EB-ZnO** samples, the E_f of **EB-ZnO** samples shifts above the CB (i.e., the **EB-ZnO** samples are degenerated) from the UPS data. Given both optical properties (the red shift of PL spectra and bandgap broadening) and UPS data, the **EB-ZnO** samples seem to be heavily n-type doped ZnO. Although N-doped ZnO with N–Zn bonds is known as p-type, in our study, n-type doping of **EB-ZnO** can be explained by (1) the zinc interstitial and oxygen vacancy as the donor result in band tails, which merge with the CB and cause band broadening,[23] or (2) N–C bonds, such as amine groups,
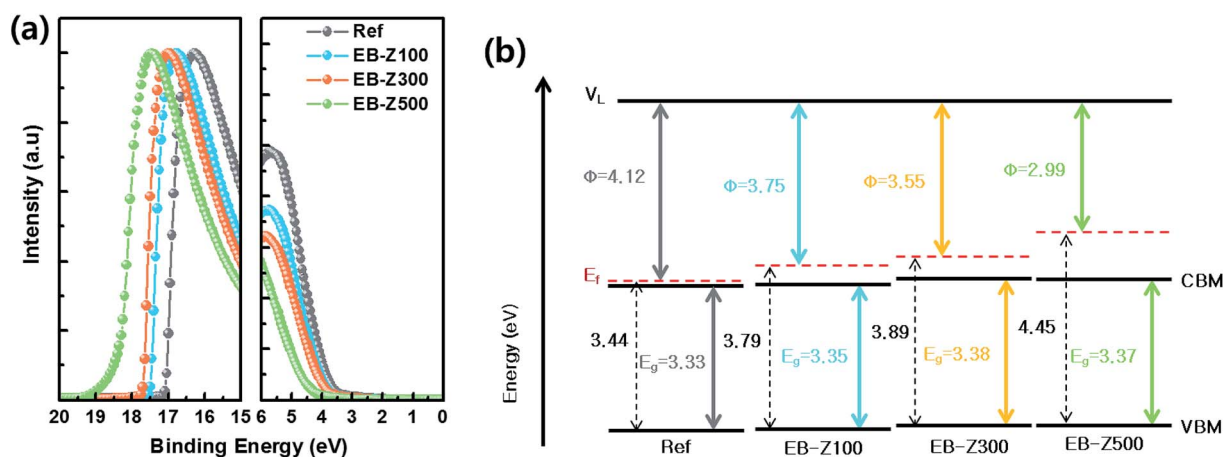

Fig. 4 (a) UPS data and (b) corresponding energy diagram of **Ref**, **EB-Z100**, **EB-Z300** and **EB-Z500**.

adsorbed on the surface can influence the reduction of W.F due to the interfacial dipole, similarly to the previously reported result.[30] Unfortunately, in our study, the electron mobility and hole measurement of the **Ref** and **EB-ZnO** samples could not be measured probably due to the highly resistive films.

Photovoltaic properties

The photovoltaic properties of the samples were investigated with the device structure of ITO/**EB-ZnO**/PTB7-Th:PC$_{71}$BM/MoO$_3$/Ag. The J–V characteristic in a single batch and the average of photovoltaic performance parameters are shown in Fig. 5a–c and Table 3. For the **Ref** samples, the open circuit voltage (V_{oc}), short circuit current density (J_{sc}), fill factor (FF) and PCE values were 0.79 V, 15.92 mA cm^{-2}, 64.3% and 8.05%, respectively. When **EB-Z100** and **EB-Z300** were used, the PCE was significantly enhanced, and the device with **EB-Z100** shows the best performance with an FF of 71.8% and PCE of 9.36% (increase of 13%). From the modified W.F, we expected that **EB-Z500** would show the best results because the W.F of the samples decreases with the increase in irradiation dose. Interestingly, **EB-Z500** shows the lowest PCE and widest distribution of PCE. The external quantum efficiency (EQE) of the same devices is shown in Fig. 5d. The measured J_{sc} is less than the

value calculated from the EQE data (the error is less than 10%). This discrepancy can be due to the difference in illumination conditions.[31]

Given the average performance parameters, there is no difference in V_{oc}, whereas the tendency of FF is the same as that of PCE. The V_{oc} is mainly determined by the energy level difference between the highest occupied molecular orbital (HOMO) of the donor and the lowest unoccupied molecular orbital (LUMO) of the acceptor and the work function difference of two metals. However, our result shows that the V_{oc} does not change, which is because the band bending between the low conductivity ZnO and organic layers may not be significant. From Table 3 and Fig. 5e, the series resistance (R_s) for the devices with **Ref** and **EB-Z100** is similar, whereas R_s for the device with **EB-Z300** and **EB-Z500** increases, and the shunt resistance (R_{sh}) for the device with **EB-Z100** increases, whereas R_{sh} for the devices with **EB-Z300** and **EB-Z500** decreases; and for all the samples, there is a difference in R_{sh} but it is not significantly large because it is not one order of magnitude, except for **EB-Z100**. The reduction in R_s and increase in R_{sh} for **EB-Z100** may reduce the leakage current and charge transport barrier and suppress the charge recombination,[32] thus resulting in high FF and PCEs.
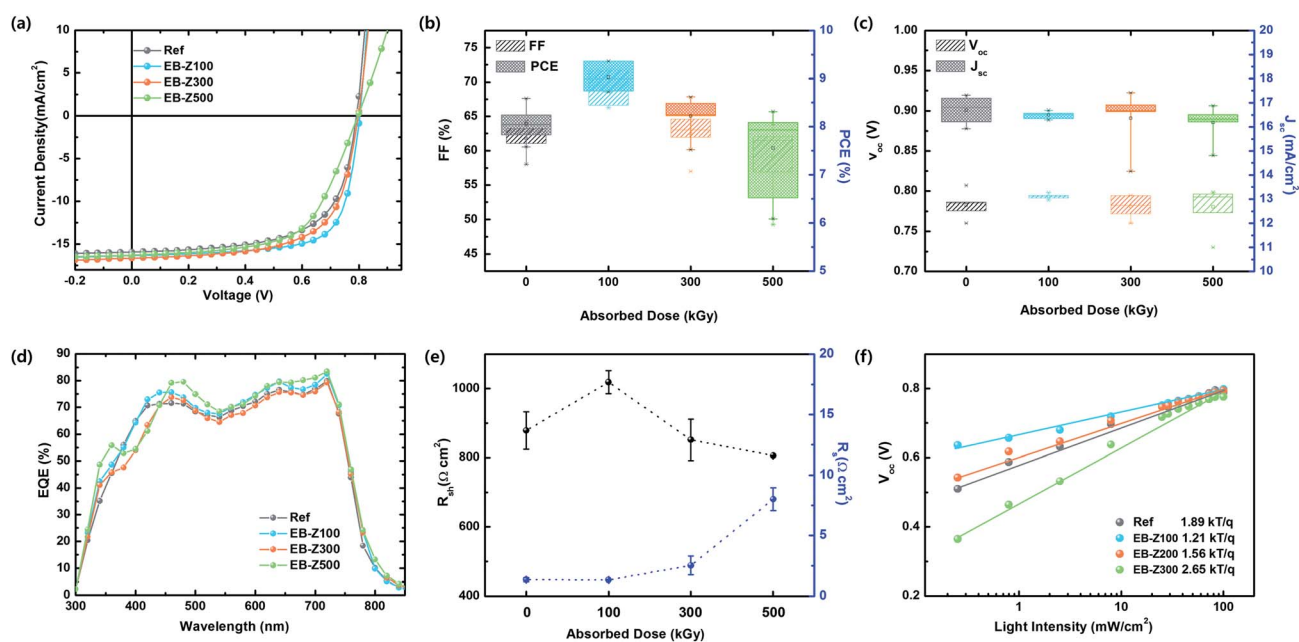

Fig. 5 (a) J–V curve, (b) variation in FF and PCE, (c) variation in V_{oc} and J_{sc}, (d) corresponding EQE data, (e) R_s and R_{sh}, and (f) V_{oc} dependence on P_{light} for the PSCs based on ITO/**Ref** and **EB-ZnO**/PTB7-Th:PC$_{71}$BM/MoO$_3$/Ag.

Table 3 The photovoltaic parameters of the devices shown in Fig. 5a and measurements from 8 PSC devices based on ITO/**Ref** and **EB-ZnO**/PTB7-Th:PC$_{71}$BM/MoO$_3$/Ag

Sample	V_{oc} (V)	J_{sc} (mA cm^{-2})	FF (%)	PCE (%)	EQE J_{sc} (mA cm^{-2})	R_s (Ω cm^2)	R_{sh} (Ω cm^2)
Ref	0.79 (0.78 ± 0.02)	15.92 (16.69 ± 0.6)	64.3 (61.8 ± 2.4)	8.05 (7.93 ± 0.3)	17.50	1.35 ± 0.15	878 ± 54
EB-Z100	0.80 (0.79 ± 0.01)	16.35 (16.49 ± 0.2)	71.8 (69.1 ± 2.4)	9.36 (8.93 ± 0.3)	18.03	1.33 ± 0.06	1018 ± 33
EB-Z300	0.79 (0.78 ± 0.01)	16.67 (16.36 ± 1.3)	65.2 (62.0 ± 3.0)	8.62 (8.16 ± 0.5)	17.24	2.53 ± 0.77	851 ± 60
EB-Z500	0.80 (0.78 ± 0.03)	16.27 (16.17 ± 0.7)	61.2 (61.1 ± 5.4)	7.93 (7.47 ± 0.9)	18.23	8.00 ± 0.95	806 ± 0.2

The results for **EB-Z100** can be ascribed to (1) energetically favorable electron transporting[29] from $PC_{71}BM$ to **EB-Z100** due to the energy level offset between the LUMO of $PC_{71}BM$ (about 3.9 eV) and up shifted E_f (W.F = 3.75 eV), which is attributed to Zn_i and V_O, (2) smoother surface (root mean square (RMS): 0.698 nm), which enables good contact with the active layer, and (3) reduced surface hydroxyl groups, which can trap electrons and holes. Although **EB-Z300** shows a lower R_{sh} and higher R_s, its PCE and FF is better, compared with that of the **Ref** sample, and its results are complicated due to its lower work function, slightly rough surface (rms: 0.943 nm) and various defects. **EB-Z500** shows the worst result with the largest R_s and lowest R_{sh} which can result from its roughest surface (rms: 3.939 nm) inducing bad contacts with the active layer. Despite the reduced surface hydroxyl groups of **EB-Z500**, another reason for its poor results can be that it is too heavily doped ZnO due to the increase in Zn_i, which leads to an increase in charge recombination. In our study, Zn_i and V_O resulted in appropriately degenerated (doped) ZnO for better energy transfer in solar cells below 500 kGy. The correlation between defects and device performance is very complicated due to simultaneous presence of various defects.

To understand the nature of charge carrier recombination, we investigated the light intensity (P_{light}) dependence of V_{oc}, which enables bimolecular and trap-assisted recombination[32,33] to be distinguished in Fig. 5d. The slope (S) of V_{oc} versus the logarithm of P_{light} indicates the presence of trap-assist recombination; and the S value is 1.89, 1.21, 1.56 and 2.65 kT q^{-1} for **Ref**, **EB-Z100**, **EB-Z300** and **EB-Z500**, respectively. This trend is not exactly matched to the trend of R_{sh}; however, the lowest S of **EB-Z100** (S nearly equal to kT q^{-1}) is consistent with the lowest R_s and this result contributes to the dominant bimolecular recombination, whereas the highest S of **EB-Z500** is also consistent with the highest R_{sh}, thus trap-assisted recombination is expected to be dominant. Although the trend of resistance (R_s and R_{sh}) of **EB-Z300** is not matched to the FF and PCEs, its smaller S, which indicates the reduction of charge recombination, can explain the PCE value. Therefore, **EB-ZnO** as a CIL is beneficial to reduce charge recombination in polymer solar cells.

Conclusions

In conclusion, we demonstrated an efficient and simple method to obtain modified sol–gel ZnO films by irradiating the sol–gel ZnO precursor solution with an electron beam. The photovoltaic performance of the device based on **EB-ZnO** is dependent on irradiation dose. The enhancement in the photovoltaic performance of the device based on **EB-ZnO** is mainly due to (1) lower work function, which is attributed to degenerated n-type ZnO by donors such as Zn_i and V_O, (2) reduced surface hydroxyl groups, and (3) smooth surface, which lead to efficient electron transfer and low leakage current. As a result, the PCE of the device with **EB-Z100** achieved 9.36% with a 16% increment, compared with 8.05% for **Ref**. Most importantly, we demonstrate the feasibility of enhancing the efficiency of inverted polymer solar cells by using modified sol–gel ZnO films, which

are obtained by irradiating sol–gel ZnO solutions with an electron beam, and that this approach can be a simple method for manufacturing modified sol–gel ZnO.

References

1 Q. Wan, X. Guo, Z. Wang, W. Li, B. Guo, W. Ma, M. Zhang and Y. Li, *Adv. Funct. Mater.*, 2016, **26**, 6635.

2 Y. Liu, J. Zhao, Z. Li, C. Mu, W. Ma, H. Hu, K. Jiang, H. Lin, H. Ade and H. Yan, *Nat. Commun.*, 2014, **5**, 5293.

3 S. Holliday, R. S. Ashraf, A. Wadsworth, D. Baran, S. A. Yousaf, C. B. Nielsen, C. Tan, S. D. Dimitrov, Z. Shang and N. Gasparini, *Nat. Commun.*, 2016, **7**, 11585.

4 Y. Lin, J. Wang, Z. G. Zhang, H. Bai, Y. Li, D. Zhu and X. Zhan, *Adv. Mater.*, 2015, **27**, 1170.

5 H. Zhou, Y. Zhang, C. K. Mai, S. D. Collins, G. C. Bazan, T. Q. Nguyen and A. J. Heeger, *Adv. Mater.*, 2015, **27**, 1767.

6 J. Huang, C. Z. Li, C. C. Chueh, S. Q. Liu, J. S. Yu and A. K. Y. Jen, *Adv. Energy Mater.*, 2015, **5**, 1500406.

7 B. Walker, H. Choi and J. Kim, *Curr. Appl. Phys.*, 2017, **17**, 370.

8 R. Kang, S. H. Oh and D. Y. Kim, *ACS Appl. Mater. Interfaces*, 2014, **6**, 6227.

9 I. Etxebarria, A. Guerrero, J. Albero, J. G. Garcia-Belmonte, E. Palomares and R. Pacios, *Org. Electron.*, 2014, **15**, 2756.

10 S. Nho, G. Baek, S. Park, B. Lee, M. Cha, D. Lim, J. Seo, S. H. Oh, M. S. Song and S. Cho, *Energy Environ. Sci.*, 2016, **9**, 240.

11 W.-Y. Jin, R.-T. Ginting, S.-H. Jin and J.-W. Kang, *J. Mater. Chem. A*, 2016, **4**, 3784.

12 Z. Liang, Q. Zhang, L. Jiang and G. Cao, *Energy Environ. Sci.*, 2015, **8**, 3442.

13 B. I. Kharisov, O. V. Kharissova and U. Mendez, *Radiation Synthesis of Materials and Compounds*, CRC Press, 2013, ch. 4, pp. 81–83.

14 N. S. Kown, C. H. Jung and S. I. Na, *Org. Electron.*, 2016, **34**, 67.

15 K. B. Sapnar, V. N. Bhoraskar, S. D. Dhole, L. A. Ghule and K. M. Garadkar, *Effects of 6 MeV Electron Irradiation on ZnO Nanoparticles Synthesized by Microwave Method. Proceedings of 2011 Particle Accelerator Conference*, New York, NY, USA, 2011, pp. 2166–2168.

16 J. S. Bhat, A. S. Patil, N. Swami, B. G. Mulimani, B. R. Gayathri, N. G. Deshpande, G. H. Kim, M. S. Seo and Y. P. Lee, *J. Appl. Phys.*, 2010, **108**, 043513.

17 Y. Sun, J. H. Seo, C. J. Takacs, J. Seifter and A. J. Heeger, *Adv. Mater.*, 2011, **23**, 1679.

18 Q. Zhu, C. Xie, H. Li, C. Yang, S. Zhang and D. Zeng, *J. Mater. Chem. C*, 2014, **2**, 4566.

19 F. Kayaci, S. Vempati, I. Donmez, N. Biyikli and T. Uyar, *Nanoscale*, 2014, **6**, 10224.

20 F. Guo, W. Shi, W. Guan and Y. Liu, *Sep. Purif. Technol.*, 2017, **173**, 295.

21 Y. Yoon, M. Kwon, B. C. Lee and J. W. Kang, *J. Adv. Oxid. Technol.*, 2012, **15**, 301.

22 Y. J. Choi, K. M. Kang and H. H. Park, *Sol. Energy Mater. Sol. Cells*, 2015, **132**, 403.

23 H. P. He, Z. Wang, H. F. Duan and Z. Z. Ye, *Phys. Chem. Chem. Phys.*, 2015, **17**, 17552.

24 T. Makino, Y. Segawa, S. Yoshida, A. Tsukazaki, A. Ohtomo and M. G. Kawasaki, *Appl. Phys. Lett.*, 2004, **85**, 759.

25 K. Lim, M. A. A. Hamid, R. Shamsudin, N. H. Al-Hardan, I. Mansor and W. Chiu, *Materials*, 2016, **9**, 300.

26 F. Kayaci, S. Vempati, I. Donmez, N. Biyikli and T. Uyar, *Nanoscale*, 2014, **6**, 10224.

27 S. Vempati, J. Mitra and P. Dawson, *Nano Res. Lett.*, 2012, **7**, 470.

28 L. X. Zhang, J. H. Zhao, H. Q. Lu, L. Li, J. F. Zheng, J. Zhang, H. Li and Z. P. Zhu, *Sens. Actuators, B*, 2012, **171–172**, 1101.

29 L. Zuo, S. Zhang, S. Dai and H. Chen, *RSC Adv.*, 2015, **5**, 49369.

30 Y. Zhou, C. Fuentes-Hernandez, J. Shim, J. Meyer, A. J. Giordano, H. Li, P. Winget, T. Papadopoulos, H. Cheun, J. Kim, M. Fenoll and A. Dindar, *Science*, 2012, **336**, 327.

31 E. Zimmermann, P. Ehrenreich, T. Pfadler, J. A. Dorman, J. Weickert and L. Schmidt-Mende, *Nat. Photonics*, 2014, **8**, 669.

32 J. S. Yeo, M. J. Kang, Y. S. Jung, R. Kang, S. H. Lee, Y. J. Heo, S. H. Jin, D. Y. Kim and S. I. Na, *Nano Energy*, 2016, **21**, 26.

33 C. M. Proctor and T.-Q. Nguyen, *Appl. Phys. Lett.*, 2015, **106**, 083301.

34 X. Zhang, J. Qin, Y. Xue, P. Yu, B. Zhang, L. Wang and R. Liu, *Sci. Rep.*, 2014, **4**, 4596.

35 Z. Liang, Q. Zhang, L. Jiang and G. Cao, *Energy Environ. Sci.*, 2015, **8**, 3442–3476.

This journal is © The Royal Society of Chemistry 2017